Catalysis Today 158 (2010) 44–55

Contents lists available at ScienceDirect

Catalysis Today

journal homepage: www.elsevier.com/locate/cattod

Preferential oxidation of CO in H_2 rich stream (PROX) over gold catalysts supported on doped ceria: Effect of preparation method and nature of dopant

Lyuba Ilieva [a,*], Giuseppe Pantaleo [b], Ivan Ivanov [a], Andreana Maximova [a], Rodolfo Zanella [c], Zbigniew Kaszkur [d], Anna Maria Venezia [b], Donka Andreeva [a]

[a] Institute of Catalysis, Bulgarian Academy of Sciences (BAS), "Acad. G. Bonchev" str., bl.11, 1113 Sofia, Bulgaria
[b] Istituto per lo Studio di Materiali Nanostrutturati, CNR, I-90146 Palermo, Italy
[c] Centro de Ciencias Aplicadas y Desarrollo Tecnológico, Universidad Nacional Autónoma de México, Circuito Exterior S/N, Ciudad Universitaria, C.P. 04510 México D.F., Mexico
[d] Institute of Physical Chemistry, PAS, Kasprzaka 44/52, 01-224 Warszawa, Poland

ARTICLE INFO

Keywords:
PROX
Gold
Ceria modified with FeO_x
MnO_x or CoO_x

ABSTRACT

The reaction of PROX over nanosized gold catalysts, supported on ceria doped with FeO_x, MnO_x and CoO_x, was investigated. The modified ceria supports were synthesized by co-precipitation (CP) and by mechanochemical activation (MA). The catalysts were characterized by XRD, HRTEM and TPR. When the CP preparation method was applied a deeper insertion of dopant in ceria structure occurs, while with the MA the formation of separate dopant oxide phases occurs (XRD and HRTEM data). On the basis of TPR results the most probable oxidative state of dopant ions was suggested. The catalytic test showed that gold catalysts on MA ceria supports, modified with FeO_x and MnO_x, can be selected as the most promising ones for PROX among the studied catalysts. The obtained differences in catalytic behaviour cannot be related to the effect of gold because using both preparation modes a high dispersion of gold particles was evidenced by HRTEM. The reason could be searched in the support structure and properties depending on the dopant nature and on the preparation method. In the case of MA technique, beside gold on ceria (modified with Fe and Mn), the gold on separate FeO_x and MnO_x phases could also contribute to the high PROX activity and selectivity. On the contrary, the presence of Co_3O_4 phase could be the reason for the low catalytic activity and selectivity observed with Co-containing gold catalyst, prepared by MA.

1. Introduction

Proton exchange membrane (PEM) fuel cells, powered by hydrogen, offer a new approach to the control of vehicle emissions. To avoid poisoning the anodes of fuel cells, the level of CO concentration must be below 10 ppm for Pt anodes and below 100 ppm for CO-tolerant alloy anodes. One promising solution of the problem has been the preferential CO oxidation in H_2 rich stream (PROX) as a simple and economic method for the removal of CO traces. Various catalytic systems have been investigated and the efforts have been focused on choosing catalysts and operating conditions that minimize the oxidation of hydrogen. In order to avoid the presence of heat changes, the most convenient temperature for PROX is the fuel cell operating temperatures (80–100 °C). For this low temperature level, oxide-supported gold catalysts have been suggested as promising candidates in Ref. [1] and references therein. The rate of CO oxidation over gold has been found to exceed that of H_2 oxidation [2–4]. The higher selectivity in PROX at low temperatures of Au in comparison to Pt was explained in a theoretical study of Kandoi et al. [5] showing that over gold a lower barrier for CO oxidation than that for H_2 exists. The activity of gold-containing catalysts is known to be sensitive to the size of the gold particles, the gold–support interface and the interactions between the gold and the support, the preparation conditions, the nature of the support. It is the latter effect that has attracted most recent attention. The essential role of the reducible transition metal oxides as carriers is considered not only as supports for nanosized gold particles but also to provide large amount of highly mobile oxygen species being able to react with CO [2,6–8]. Among the supports for gold catalysts being able to activate and supply oxygen, Fe_2O_3 [6,9–16], MnO_x [3,15,17–19] and Co_3O_4 [2,11] have been studied in low temperature CO oxidation in the absence or presence of excess H_2. Many PROX studies have been focused on the gold supported on ceria because of the high oxygen capacity of CeO_2 as well as its ability of small gold particles stabilization [7,11,20–25]. Schubert et al. have established that Au/CeO_2 and, in particular, Au/Fe_2O_3 represented the best compromise regarding the PROX activity, selectivity and long term stability under the applied conditions of simulated methanol reformate [11]. Chang and co-authors have reported that the co-existence of metallic and oxidized gold species supported on ceria seems

* Corresponding author. Tel.: +359 29792572; fax: +359 29712967.
E-mail address: luilieva@ic.bas.bg (L. Ilieva).

0920-5861/$ – see front matter © 2010 Elsevier B.V. All rights reserved.
doi:10.1016/j.cattod.2010.06.017

to be the main reason for the higher activity in CO oxidation of Au/CeO_2 with respect to Au/MnO_x [26] as well as a high PROX activity of Au/MnO_2–CeO_2 catalyst due to the synergistic effects of MnO_2–CeO_2 composite oxides prepared by impregnation [27]. Tu et al. obtained a significant improvement of selectivity in PROX over ultrasonically pre-treated Au/MnO_x–CeO_2 catalyst, due to the suppression of the H_2 dissociation [28]. PROX over Au/CeO_2–Co_3O_4 has been studied by Wang et al. [29] and the possible explanation concerning catalysts' deactivation was proposed [30]. It is known that the addition of ions with oxidation state differing from (4+) to ceria causes the formation of a defective fluorite structure with increased oxygen mobility [31]. Very recently, PROX over Au on CeO_2 doped by Sm, La, and Zn has been studied in Refs. [32,33]. The results obtained by some of us [34] showed that gold catalysts supported on modified with rare earths ceria using co-precipitation method of supports preparation manifested higher activity and selectivity in PROX compared to those on mechanochemically prepared supports. The most promising catalyst contained yttrium as a dopant.

In the present study nanosized gold catalysts supported on ceria doped with MeO_x (MeO_x = FeO_x, MnO_x and CoO_x) are investigated. The modified ceria supports were synthesized by different methods: co-precipitation (CP) or mechanochemical activation (MA). Unlike the previously studied gold on ceria modified by rare earths, the modifying ions are characterized by changeable oxidative state. The above mentioned literature references have shown that the chosen reducible dopants are catalytically active and selective in the reaction of PROX. The paper is focused on the comparison of the size of gold particles, structure and properties of the supports, and the catalytic activity and selectivity in the reaction of PROX. The dependence on the nature of the dopant and the applied preparation method is commented.

2. Experimental

2.1. Catalyst preparation

Two methods were applied for the preparation of the modified ceria supports: (i) co-precipitation (the samples were denoted as CP) from a solution of $Ce(NO_3)_3$ and corresponding nitrates of the dopants ($Fe(NO_3)_3$, $Co(NO_3)_2$ or $Mn(NO_3)_2$) in appropriate ratio (the amount of MeO_x was 10 wt%) with a solution of K_2CO_3 at constant pH = 9.0 and temperature = 60 °C. The resulting precipitates were aged at the same temperature for 1 h, then filtered and washed until removal of NO_3^- ions. The washed precipitates were dried in vacuum at 80 °C and calcined under air at 400 °C for 2 h; (ii) mechanochemical activation (the samples were denoted as MA) using a freshly prepared vacuum-dried cerium hydroxide and the oxide of the dopant: Fe_2O_3, Co_3O_4 or MnO_2. The cerium hydroxide was obtained by precipitation of cerium nitrate with a solution of K_2CO_3. A mixture of cerium hydroxide and the corresponding dopant oxide was subjected to the mechanochemical activation by milling for 30 min in a mortar and calcination at 400 °C for 2 h. Then, before deposition of gold, the modified ceria support was activated in Ultrasonic UD-20 automatic UV disintegrator under vigorous stirring.

For comparison undoped ceria was laboratory-made by precipitation of $Ce(NO_3)_3{\cdot}6H_2O$ with K_2CO_3 (60 °C, pH 9.0). The precipitate was aged, filtered, washed, dried in vacuum at 80 °C and calcined under air at 400 °C for 2 h.

Gold (3 wt%) was added by deposition–precipitation method. It was loaded as $Au(OH)_3$ on the corresponding modified ceria support, preliminary suspended in water, through the precipitation of $HAuCl_4{\cdot}3H_2O$ with K_2CO_3 under continuous stirring at constant pH = 7.0 and temperature of 60 °C. After 1 h of ageing, filtering and careful washing, the precursors were dried under vacuum at 80 °C and calcined in air at 400 °C for 2 h. The samples were denoted as AuCeFe, AuCeMn and AuCeCo, CP or MA, correspondingly. Gold on undoped ceria was labelled as AuCe.

All syntheses were carried out in a "Contalab" automated laboratory reactor enabling careful control of all the variables (pH, temperature, stirrer speed, reactant feed flow, etc). "Analytical grade" chemicals were used for the samples preparation.

2.2. Catalyst characterization

The BET surface area of the samples was determined on a Micromeritics 'Flow Sorb II-2300' instrument with 30% N_2, 70% He mixture at atmospheric pressure and N_2 boiling temperature.

The X-ray diffraction measurements were performed using Siemens D5005 diffractometer (Bruker-AXS), Cu sealed tube operating at 40 kV and 40 mA and scintillation detector. All measured reflections were subjected to Williamson–Hall Plot analysis [35] providing reasonable linear fit and the most likely values of ceria crystallite size and microstrain parameter. The lattice constant of ceria phase for a measured ceria catalyst was estimated on the basis of linear extrapolation of its values from 11 observed reflections versus cosine of the Bragg angle to the value of the cosine equal to zero. This is a commonly used method to obtain a precise value of the parameter. For the CP samples this extrapolation cannot be done due to a high non-linearity of this diagram and significant scatter of the lattice parameter value obtained from different peaks. A careful analysis of the patterns allowed to correlate the scatter with a high strain determined from Williamson–Hall plot and a high value of Debye–Waller parameter determined from the rate of peak intensities attenuation with a scattering angle. The lattice constant scatter has been thus attributed to anisotropic strain. There are studies available in the literature suggesting the doped ceria system to be heavily strained and that associated defects might cluster in ordered arrangements [36] which can cause further anisotropy.

As microstrain for CP samples causes significant shifts of the diffraction peak position of unpredictable value, for the determination of the lattice parameter we propose the following procedure. For the samples prepared via MA route, where the lattice parameter extrapolation works reasonably well, we accept their result as the real lattice constant. For the samples prepared via CP route the highest angle peaks give the minimum scatter of the lattice parameter. The extrapolation cannot be reasonably done but these highest angle parameter values can be compared to the analogous value for the MA samples. On this basis we determine the difference that we finally add to the lattice constant determined for the MA sample arriving at the estimated value for the CP samples. The method is approximate but can provide values close to real ones provided the diffractometric errors were similar for all the samples.

High resolution transmission electron microscopy (HRTEM) and High angle annular dark field (HAADF) observations of the catalysts were performed in a JEM 2010 FasTem analytical microscope equipped with a Z-contrast annular detector. The histograms of the metal particle sizes were established from the measurement of more than 700 particles obtained by Z-contrast and Thermal Diffuse Scattering (TDS) observations.

TPR measurements were carried out by means of an apparatus described elsewhere [37]. A cooling trap (−40 °C) for removing water formed during reduction was mounted in the gas line prior to the thermal conductivity detector. H_2–Ar mixture (10% H_2), dried over a molecular sieve 5 Å (−40 °C), was used to reduce the samples at a flow rate of 24 mL min^{-1}. The temperature was linearly raised at a rate of 15 degree min^{-1}. The sample mass used was 0.05 g. It was selected by the criterion proposed by Monti and Baiker [38]. The hydrogen consumption (HC) during the reduction processes was calculated using preliminary calibration of the

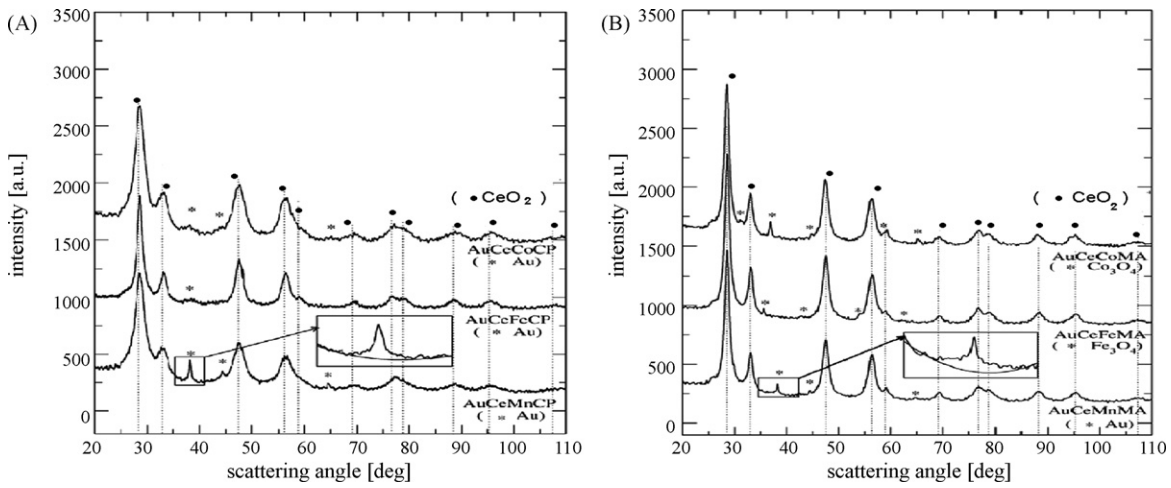

Fig. 1. X-ray diffraction spectra of gold catalysts supported on modified ceria: (A) prepared by CP method and (B) prepared by MA technique. Close up of the 1 1 1 peaks of gold is presented for AuCeMnMA and AuCeMnCP samples.

detector, performed by reducing different amounts of NiO to Ni^0 (NiO—"analytical grade" of purity, calcined for 2 h at 800 °C in order to avoid the nonstoichiometry).

2.3. Catalytic measurements

The catalytic activity and selectivity measurements in PROX over the studied gold catalysts were carried out using a quartz glass U-shaped reactor, equipped with a temperature programmed controller. The total gas inlet was 50 mL min^{-1}, containing 50% H_2 + 0.3% CO + 0.3% O_2 and He as balance (WHSV of 60,000 mL g^{-1} h^{-1}). The CO conversion and the selectivity were calculated using an ABB infrared analyzer detector for CO and CO_2 and an ABB paramagnetic Magnos206 for the O_2. The CO converted was calculated on the basis of the CO_2 produced whereas the selectivity was calculated according to the following equation:

$$S = \frac{\text{ppm}\,CO_2^{out}}{2 \times (\text{ppm}\,O_2^{in} - \text{ppm}\,O_2^{out})} \times 100 \quad (\text{in} \quad \%)$$

The preliminary test showed that the catalytic activity is a little higher using oxidative in comparison to the reductive pretreatment. By this reason, before the catalytic measurements, the samples were treated in a flow of O_2 (5 vol%) in Ar during 30 min at 150 °C.

3. Results

3.1. Catalyst characterization

The X-ray diffraction spectra of gold catalysts supported on ceria doped by FeO_x, MnO_x or CoO_x are shown in Fig. 1: (A) synthesized by CP method and (B) prepared by MA technique. For both kinds of samples, the CeO_2 diffraction lines typical of fluorite type structure can be seen. Double phases were observed with AuCeFeMA and AuCeCoMA catalysts—in addition to ceria, the lines of oxides of the corresponding dopants are also visible.

In Table 1 are presented the BET surface area, the lattice parameters (lattice constant *a* and microstrain parameter *b*) and the average particle size of ceria determined by XRD. It is seen that the BET surface area of the studied gold catalysts is of the order of 82–95 m^2 g^{-1}, except the lower value for AuCeCoCP sample. The values of lattice parameters *a* show a bigger contraction of ceria lattice for CP catalysts containing Fe and Co compared to the corresponding MA ones. The extent of the lattice constant scattering for all peaks is correlated with the strain parameter (the higher strain—the higher scattering). This is in agreement to the effect of preparation method. Co-precipitation is leading to deeper insertion of dopant in ceria structure and formation of oxygen vacancies, while predominantly surface modification is caused by mechanochemical mode. Equal *a* parameters were obtained with CP and MA catalysts containing Mn. The peak broadening strain *b* is also similar for both preparation routes. The explanation could be connected to the fact that Mn can easily enter the octahedral, ceria-type oxygen arrangement as in MnO_2 crystal pyrolusite of the same stoichiometry as CeO_2 (the very probable oxidative state of the predominant part of dopant ions incorporated in CeO_2 is Mn^{4+} as estimated below for AuCeMnCP by TPR). The addition of Fe and Co leads to a defective structure of ceria caused by oxygen vacancies formation (anions with oxidative state different from Ce^{4+}) and different ionic radii (Fe–O and Co–O bonds different from Ce–O one). In the case of Mn insertion by CP, the vacancy formation is less probable (the same oxidative state of Mn^{4+} and Ce^{4+}), and the defects in ceria structure have different characters, only due to the

Table 1
BET surface area, lattice parameters (*a* and *b*) and average size of ceria evaluated by XRD, and average size of gold particles estimated by HRTEM.

Sample	S_{BET} (m^2 g^{-1})	*a* (Å)	*b*	Av. size of ceria (nm)	Av. size of gold (nm)
AuCe	108	5.411 (4)	0.010	11.3	<5[a]
AuCeFeCP	87	5.394 (7)	0.011	9.4	2.8
AuCeFeMA	90	5.404 (7)	0.007	10.1	2.9
AuCeMnCP	82	5.394 (3)	0.006	6.3	2.9
AuCeMnMA	95	5.394 (3)	0.009	10.7	2.9
AuCeCoCP	54	5.378 (3)	0.015	5.3	–
AuCeCoMA	95	5.408 (3)	0.012	12.6	–

The figures in parentheses represent the error on the last digits from linear regression.
[a] As determined in Ref. [34].

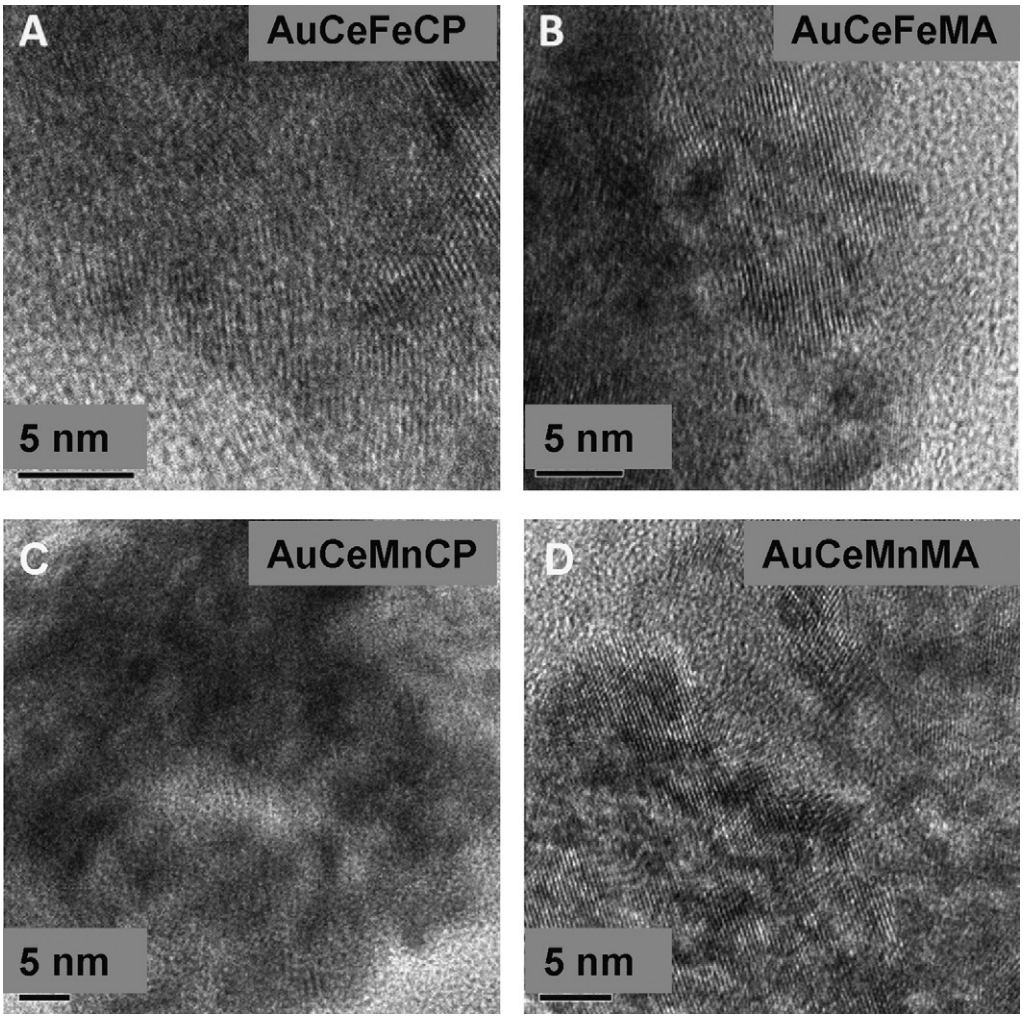

Fig. 2. HRTEM images of gold catalysts: (A) AuCeFeCP; (B) AuCeFeMA; (C) AuCeMnCP and (D) AuCeMnMA.

decreased Mn–O distance (1.88 Å in pyrolusite) compared to Ce–O one (2.343 Å). This causes, a visible increase in a Debye–Waller parameter but does not affect isotropic strain parameter.

Inserts showing close up of the 1 1 1 peaks of gold are presented in the case of diffraction patterns of AuCeMnMA and AuCeMnCP samples. The evaluation of gold crystallite size for those samples requires proper background estimation. The inserts present choices of the background line that clearly reveal two contributing modes: one broad corresponding via Scherrer formula to crystallites of 2.9 nm size; the other mode corresponds to Au crystallites of 25 nm (MA sample) and to more than 40 nm (CP sample). Assuming volume of crystallites contributing to the detected modes as being proportional to the constituent peak area, the result is: 1 large crystallite per 20,000 crystallites of 2.9 nm size for the sample MA, respectively, 1 per 2000 for the sample CP.

In Fig. 2 are illustrated the HRTEM images of Fe- and Mn-containing gold catalysts, prepared by CP or MA method. The size distribution of gold particles in these catalysts is displayed in Fig. 3: (A) AuCeFeCP, (B) AuCeFeMA, (C) AuCeMnCP, and (D) AuCeMnMA. Some differences depending on the preparation method are visible—the number of particles of 2.5 nm is the highest in both CP samples, a relatively higher number of smaller (0.5 and 1.5 nm) and higher number of particles (>2.5 nm) were registered with MA samples compared to CP ones. However, the average size of gold estimated by HAADF images was the same (2.9 nm) independent on the dopant and the method of preparation (see Table 1).

As the TEM observation encompassed about 700 crystallites for a size statistics it is reasonable to believe that the very small fraction of large crystallites (showed by XRD) in the case of Mn-containing catalysts could pass unnoticed. The detailed analysis of HRTEM and Z contrast images showed that, very rarely, big Au particles can be observed. In AuCeMnCP catalyst the biggest particle was of about 7 nm (Fig. 4A). A few big particles of 7–10 nm were found in AuCeMnMA sample (Fig. 4B). In this image, there are also two coalescing gold particles (showed by dashed arrows), the diameter of the coalesced particle (taking the longest axis) is of about 17 nm.

The analysis of the HRTEM images shows that supplementary to CeO_2, separate MeO_x phases are present in the case of MA samples. In selected HRTEM images of AuCeFeMA catalyst the existence of both Fe_2O_3 and Fe_3O_4 is illustrated (Fig. 5). The lattice parameter measured in zone A corresponds to (1 1 1), (2 2 2) and (4 0 0) reflections of Fe_3O_4 and that measured in zone B corresponds to (2 0 2), (3 0 0) and (0 0 6) reflections of Fe_2O_3 as shown in the corresponding Fast Fourier transforms (FFT). AuCeMnMA catalysts also showed separated phases of MnO_2 and Mn_2O_3 (Fig. 6). FFT of zone A shows the (4 0 0), (4 4 0) and (4 1 1) reflections of Mn_2O_3 and FFT of zone B shows the (1 1 0) reflection of MnO_2.

The TPR profiles of studied initial supports and gold catalysts are presented in Figs. 7–9. Fig. 7 shows the TPR profiles of CeO_2–FeO_x supports and the corresponding gold catalysts prepared by CP and MA method. Two TPR peaks with T_{max} at 387 and 590 °C are recorded with CeFeCP support. Concerning AuCeFeCP sample only one main peak with T_{max} at 117 °C and some high temperature

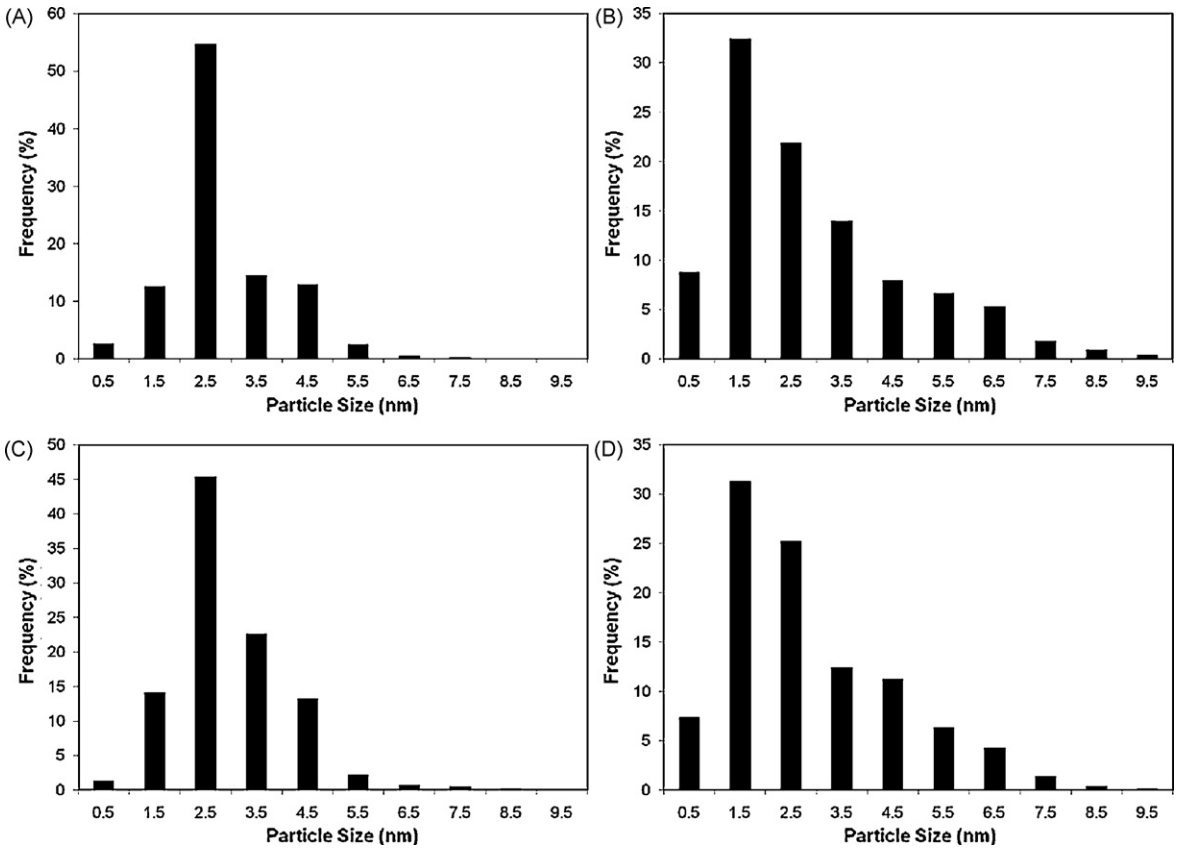

Fig. 3. Size distribution of gold particles for the studied samples: (A) AuCeFeCP; (B) AuCeFeMA; (C) AuCeMnCP and (D) AuCeMnMA.

(HT) peaks with very low intensity are visible. In the TPR pattern of CeFeMA sample three TPR peaks are presented—with T_{max} at 370, 457 and 563 °C, the HT one being the most intense. By the addition of gold a HT peak is registered at 532 °C, a low temperature (LT) LT peak at 100–120 °C appears and weak peaks at 232 and 350 °C are seen as well. It is known that ceria reduction proceeds in two steps—surface layers reduction connected to a TPR peak with maximum at about 500 °C, followed by bulk reduction at higher temperatures (above 800 °C) [39]. In the presence of gold the ceria surface layers reduction is significantly facilitated and the first TPR peak is shifted having T_{max} at 120 °C [40]. In a previous study of Au/Fe_2O_3 catalysts it was shown that the effect of gold consisted in a considerable lowering of the temperature of the reduction process $Fe_2O_3 \rightarrow Fe_3O_4$ (T_{max} = 427 for the bare support and 280 °C in the presence of gold), while the next reduction $Fe_3O_4 \rightarrow FeO \rightarrow Fe$ was not influenced (T_{max} around 600 °C) [41].

Fig. 8 represents the TPR profiles of CeO_2–MnO_x synthesized by CP or MA preparation technique and corresponding gold catalysts. Two TPR peaks with T_{max} at 298 and 457 °C are registered with CeMnCP support, while in the spectra of AuCeMnCP catalyst only

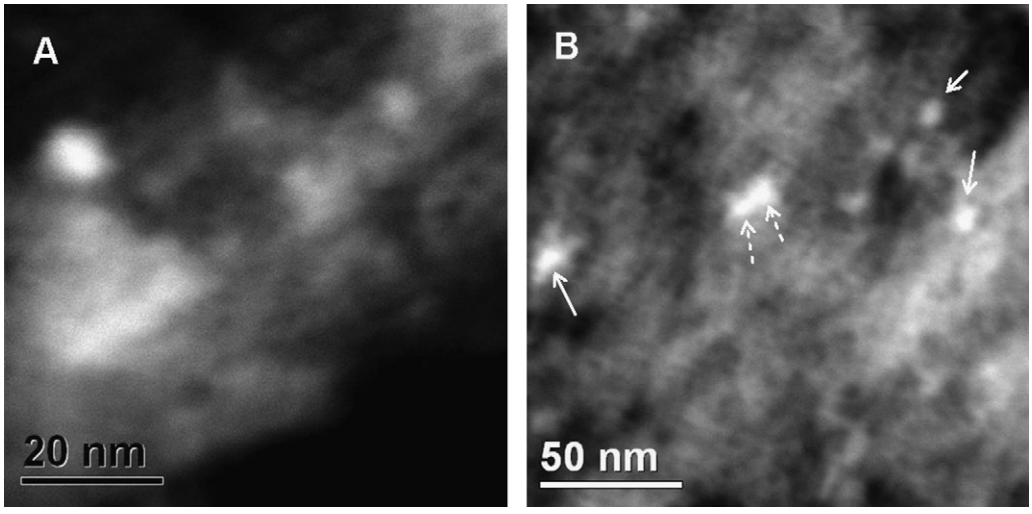

Fig. 4. Z contrast images of the samples: (A) AuCeMnCP and (B) AuCeMnMA (the Au particles are shown by arrows and the two coalescing Au particles are illustrated by dashed arrows).

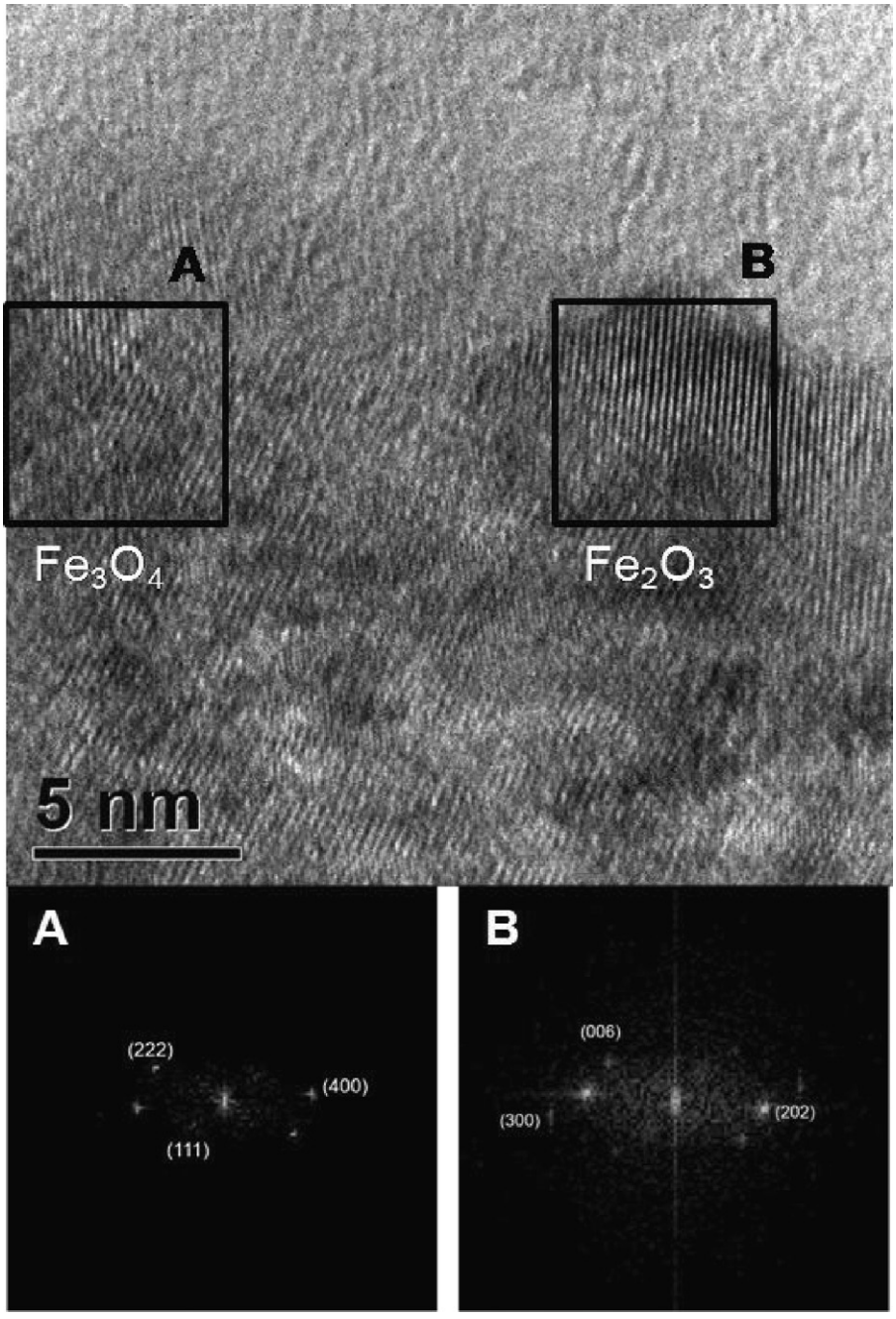

Fig. 5. HRTEM image of AuCeFeMA catalyst showing Fe_3O_4 phase in zone A and Fe_2O_3 phase in zone B with the corresponding FFT images.

one intense LT TPR peak with T_{max} = 127 °C is present. For CeMnMA sample the recorded peaks are characterized with T_{max} at 290, 442 and 495 °C. The gold loading on this supports leads to the observation of LT TPR peak with T_{max} at 85 °C and a second less intense peak at T_{max} = 292 °C. Two resolved TPR peaks with T_{max} at 291 and 419 °C were recorded during TPR of bulk MnO_2 oxide (not shown in the figure). According to the literature data the first TPR peak (T_{max} at 291 °C) is assigned to $MnO_2 \rightarrow Mn_2O_3$ [19,42] or to $MnO_2/Mn_2O_3 \rightarrow Mn_3O_4$ transition [28 and references there in], while the second one (T_{max} at 419 °C) is connected to $Mn_2O_3 \rightarrow MnO$ [19,42] or to $Mn_3O_4 \rightarrow MnO$ reduction [28 and references there in].

In Fig. 9 are displayed the TPR patterns in the case of ceria doped by CoO_x—supports and gold catalysts prepared by CP and MA method. The TPR profile of CeCoCP consists of overlapping peaks with T_{max} within the interval 145–400 °C. The spectrum of the corresponding gold catalysts (AuCeCoCP) is also complex, a LT peak at T_{max} = 112 °C appears. For the support prepared by MA method a complex TPR peak with T_{max} between 340 and 400 °C and a shoulder at 298 °C are recorded. The picture is very similar to that of the bulk Co_3O_4 spectrum (a main peak with T_{max} at 380 °C due to $CoO \rightarrow Co^0$ and a LT shoulder assigned to $Co_3O_4 \rightarrow CoO$ reduction) shown in the literature as well as in a previously performed study [43,44].

The TPR profiles are very complex because of the ability of dopants with different oxidative states being reduced in addition to ceria. On the bases of only qualitative comparison with pure oxides the exact correlation between peaks and the corresponding transitions is not possible. The evaluation of kinetic parameters of reduction characteristic for the individual reduction process is in force and it may throw more light to the TPR peaks assignment.

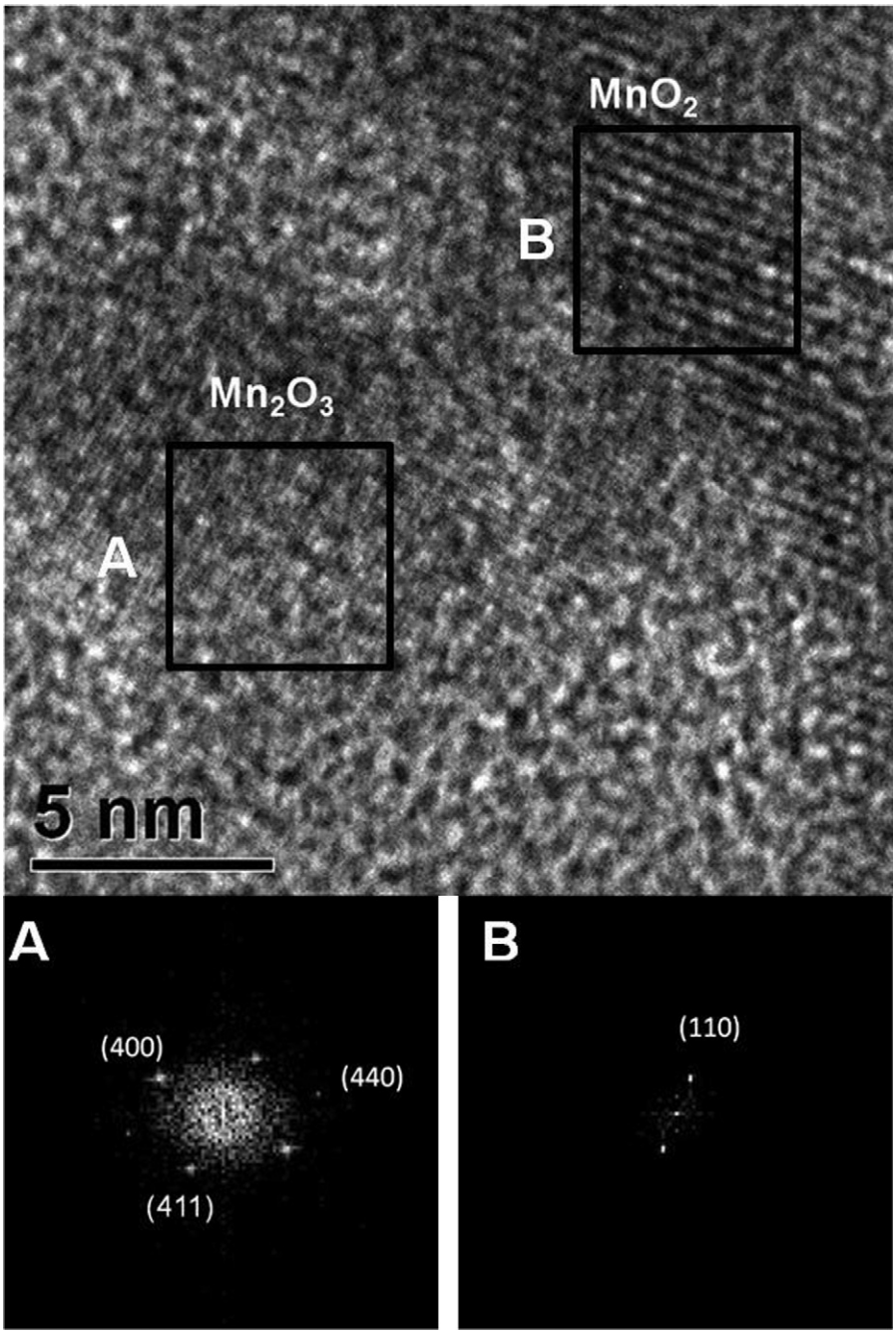

Fig. 6. HRTEM image of AuCeMnMA catalysts showing the presence of Mn_2O_3 phase in zone A and MnO_2 phase in zone B, with the corresponding FFT images.

Having in mind that the TPR profiles registered up to 650 °C (bulk ceria reduction started above this temperature) are connected to the ceria surface reduction and the reduction of dopant oxides, the evaluation of the most probable oxidative state of dopants on the bases of the calculated hydrogen consumption (HC) was carried out. The data for the initial supports are presented in Table 2. The theoretical value of HC related to ceria can be calculated taking into consideration that according to the literature data the surface layers reduction of ceria (which does not affect the fluorite structure) is limited to 17% [45] or 20% [46]. In the present case (10 wt% of the dopant oxide) the corresponding amounts of H_2 for such degrees of reduction are 0.44 and 0.52 mmol g^{-1}, respectively. The stoichiometric HC needed for the reduction of the introduced 10 wt% Fe_2O_3 to metallic Fe is 1.90 mmol g^{-1}. Therefore, the theoretical amount of HC for all reduction processes is 2.34–2.42 mmol g^{-1}. The experimentally obtain one is 2.27 mmol g^{-1} for CeFeCP sample and 2.15 mmol g^{-1} for CeFeMA one. This means that the Fe^{3+} ions are the predominant part in the support prepared by CP, while most probably some higher amount of Fe ions with lower oxidative state

Table 2
Hydrogen consumption (HC) during TPR of initial supports (temperature interval up to 650 °C).

Sample	HC (mmol g^{-1})
CeFeCP	2.27
CeFeMA	2.15
CeMnCP	1.60
CeMnMA	1.24
CeCoCP	1.76
CeCoMA	2.14

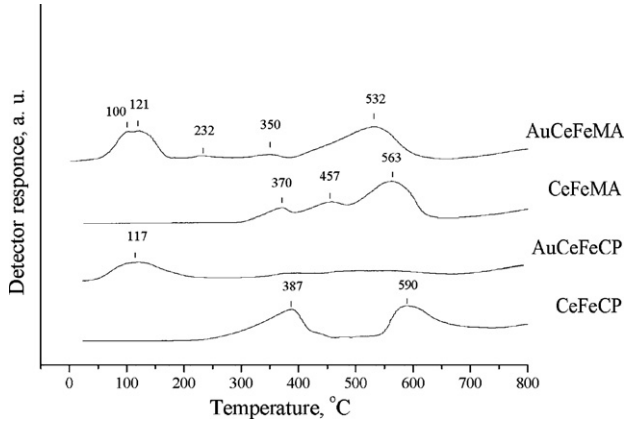

Fig. 7. TPR patterns of Fe-containing initial supports and gold catalysts.

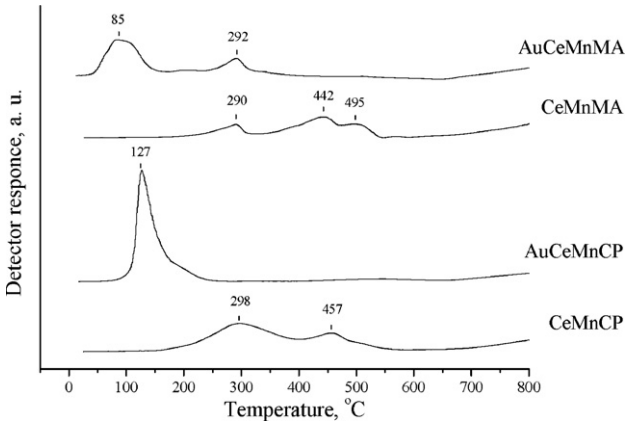

Fig. 8. TPR patterns of Mn-containing initial supports and gold catalysts.

exists in the case of MA method. The XPS analyses [47] reveal also a complex chemical nature of the dopant oxide—by XPS data Fe_2O_3 and Fe_3O_4 phases are coexisting iron phases in both CP and MA catalysts (Fe $2p_{3/2}$ XPS peaks positioned at BE equal to 712.1 ± 0.2 eV and 710.7 ± 0.1 eV for Fe_2O_3 and Fe_3O_4, respectively [48,49]).

Following the same procedure for the Mn containing supports, the theoretical amount of HC is 1.65–1.73 mmol g^{-1} in respect to ceria surface reduction and $MnO_2 \rightarrow Mn_2O_3 \rightarrow MnO$ transformation (1.21 mmol g^{-1} HC needed). Comparing to the experimental values in Table 2, it is seen that with CP support the most probable oxidative state of dopant ions is Mn^{4+}, however with MA one

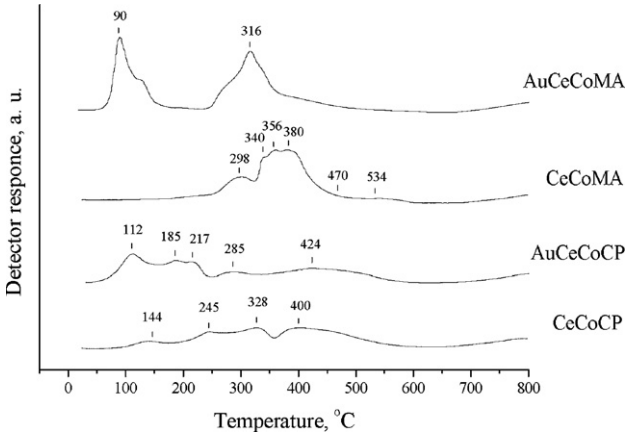

Fig. 9. TPR patterns of Co-containing initial supports and gold catalysts.

Table 3
Hydrogen consumption (HC) during TPR of gold catalysts (temperature interval up to 220 °C).

Sample	HC (mmol g^{-1})
AuCe	0.46
AuCeFeCP	0.62
AuCeFeMA	0.74
AuCeMnCP	1.67
AuCeMnMA	1.28
AuCeCoCP	0.90
AuCeCoMA	0.94

the oxidative state could not be Mn^{4+} (HC of only 1.24 mmol g^{-1}). Taking into consideration the stoichiometric HC for $Mn_2O_3 \rightarrow MnO$ reduction (0.93 mmol g^{-1}), the presence of Mn^{3+} ions could be supposed in the case of MA preparation mode. These observations were confirmed having a very good agreement with the obtained XPS results [47]—in the Mn-doped sample prepared by CP, only MnO_2 was detected (Mn $2p_{3/2}$ peak positioned at BE = 642.1 eV), while in MA catalysts both MnO_2 and Mn_3O_4 were registered (Mn $2p_{3/2}$ peaks positioned at BE = 642.7 and 641.5 eV, respectively [49]).

Close values of the theoretical (2.10–2.18 mmol g^{-1}) and experimentally obtained HC (2.14 mmol g^{-1}) are found with CeCoMA support, making the calculations in respect to the reduction of 10 wt% Co_3O_4 to metallic Co (stoichiometric HC of 1.66 mmol g^{-1}). By this reason the presence of Co^{3+} and Co^{2+} ions in a ratio closed to that in Co_3O_4 could be assumed. The confirmation is also the shape of the TPR profile of CeCoMA sample, which is very similar to that obtained with bulk Co_3O_4 [43,44]. This could mean that a bigger part of dopant is not incorporated in ceria but exists as a separate phase. Differently, CoO_x dopant cannot be considered as Co_3O_4 (1.76 mmol g^{-1}, Table 2) in respect to CP sample. Assuming the $CoO \rightarrow Co^0$ transformation as a possible reduction process (stoichiometric HC of 1.33 mmol g^{-1}), the theoretical HC for CeCoCP is 1.77–1.85 mmol g^{-1}. A comparison with the experimental value of 1.76 mmol g^{-1}, leads to a suggestion that the most probable oxidative state of cobalt in the support prepared by CP is Co^{2+}. The obtained TPR results about the most probable oxidative state of dopants were confirmed by XPS [47]—in the AuCeCoCP sample only Co^{2+} was detected (peak positioned at BE = 781.1–781.7 eV), while in AuCeCoMA Co^{3+} was registered as well (peak positioned at BE = 779.2–779.7 eV [49]).

In Table 3 the HC in the LT interval (up to 220 °C) of the studied gold containing catalysts is presented. The total HC is a result of reduction processes of dopant oxide and ceria surface layers reduction. The HC due to the partially positively charged gold could be neglected. In the case of FeO_x as dopant, taking into account the stoichiometric HC for the reduction process $Fe_2O_3 \rightarrow Fe_3O_4$ (as it was mentioned above gold does not influence the next reduction steps), it could be concluded that: in the case of MA catalyst the existed amount of Fe^{3+} are reduced with HC similar to that for hematite to magnetite transformation, while in AuCeFeCP catalysts some of the Fe^{3+} ions incorporated in ceria structure are not included in the reduction process occurring into this LT interval.

Interesting TPR results are obtained with AuCeMnCP catalyst—supplementary to ceria surface layers all reduction processes included Mn^{4+} to Mn^{2+} transformation are complete in the LT interval (one single LT TPR peak). For AuCeMnMA sample in addition to the reduction including CeO_2 surface and some amount of Mn^{4+}, the LT $Mn^{3+} \rightarrow Mn^{2+}$ formation has to occur predominantly (the above analysis of TPR data for CeMnMA support showed that the amount of Mn^{3+} is higher than that of Mn^{4+}).

For AuCeCoMA catalyst the HC, which is higher than the needed one for ceria surface layers reduction, could be connected to the reduction of Co^{3+} to Co^{2+}. The HC obtained with AuCeCoCP (Table 3) suggests that in the presence of gold the amount of Co^{3+} is higher

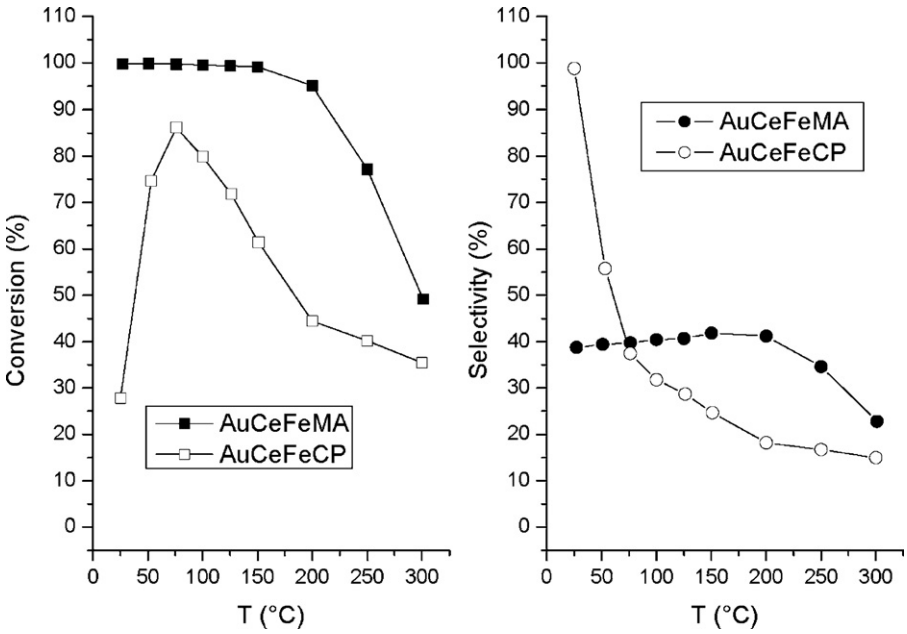

Fig. 10. Comparison between MA and CP preparation methods regarding the degree of CO conversion and selectivity over gold catalysts on doped with FeO_x ceria.

in comparison to the initial support. Some reduction to Co^0 occurs in accordance with results obtained in Ref. [43] and the catalytic test showed below (methane formation at temperature ≥150 °C for AuCeCoMA and at temperature ≥250 °C for AuCeCoCP). It is known that adding ceria to pure cobalt oxides led to the Co^{3+}/Co^{2+} ratio increasing [50]. The increase amount of Co^{3+} ions in AuCeCoCP as compared to the initial support (predominant part is Co^{2+}) could be explained by the electron transfer, enhanced by the presence of gold, from Co^{2+} incorporated in ceria, to Ce^{4+}.

3.2. Catalytic activity and selectivity

The effect of the preparation method on the catalytic activity expressed as degree of CO conversion and selectivity toward CO_2 is illustrated in Figs. 10–12. In the case of Fe as dopant (Fig. 10) the gold catalysts prepared by MA exhibited significantly higher activity than that prepared by CP. A stable activity close to 100% in the interval from room temperature up to 150 °C was registered with AuCeFeMA catalyst. Above 75 °C the selectivity of MA catalyst is higher comparing to CP one, being also stable (about 40%) up to 200 °C. It is seen in Fig. 11 that the catalytic behaviour of the two Mn-containing catalysts does not differ significantly. AuCeMnMA catalyst is highly active compared to AuCeMnCP one in the interval 100–150 °C. At 77 °C (which is of interest for fuel cell application) the MA catalyst is slightly less active than the CP one but the observed selectivity was 61%. In the studied temperature interval the MA preparation mode leads to a higher selectivity in comparison to CP method. The results of catalytic tests over Co containing samples are presented in Fig. 12. The behaviour of AuCeCoMA is very different comparing to AuCeFeMA and AuCeMnMA catalysts. In the interval 50–200 °C the PROX activity and selectivity of AuCeCoMA was significantly lower as compared to the corre-

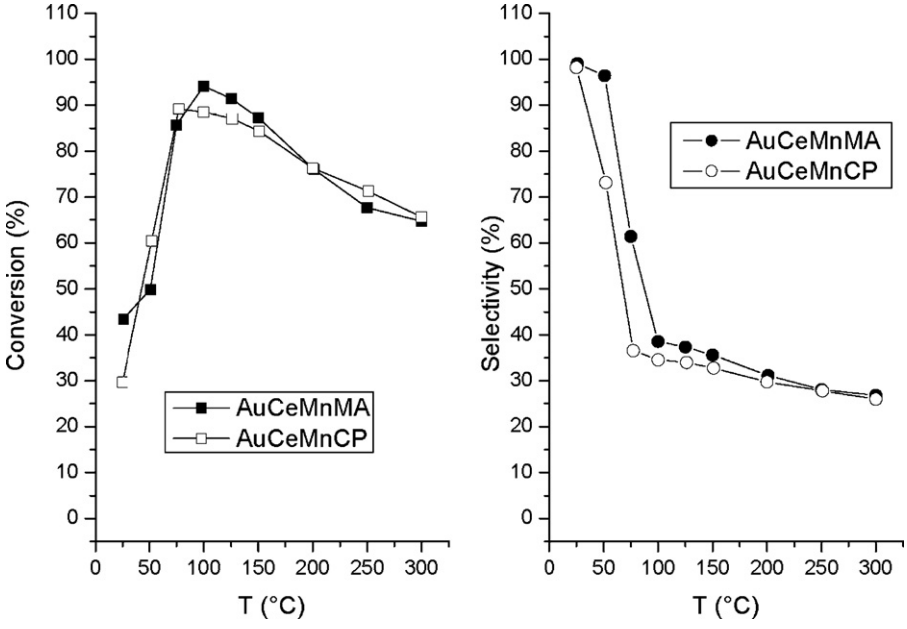

Fig. 11. Comparison between MA and CP preparation methods regarding the degree of CO conversion and selectivity over gold catalysts on doped with MnO_x ceria.

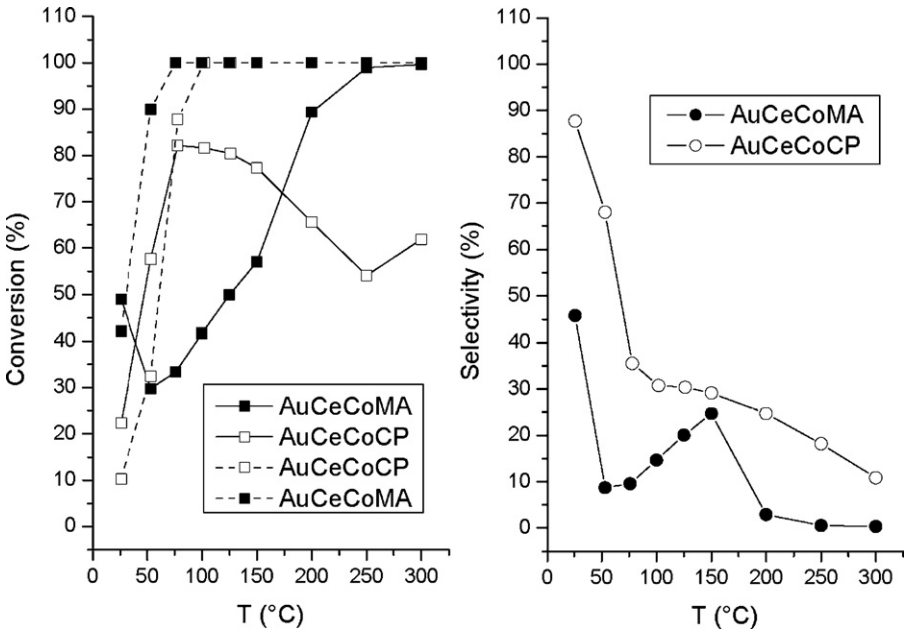

Fig. 12. Comparison between MA and CP preparation methods regarding the degree of CO conversion and selectivity over gold catalysts on doped with CoO_x ceria. The degree of O_2 conversion is given as well (dash lines).

sponding CP catalyst. Only in the case of Co as dopant the methane formation was detected: at temperature ≥150 °C with AuCeCoMA, and at temperature ≥200 °C with AuCeCoCP.

A comparison between AuCeFeMA and AuCeMnMA (both having better PROX performance than AuCeCoCP), and AuCe catalyst is shown in Fig. 13. In the temperature interval of interest (75–100 °C), the PROX activity and selectivity is higher over gold on ceria supports modified by MA method in comparison to gold on ceria.

4. Discussion

The test for catalytic activity and selectivity showed that AuCeFeMA and AuCeMnMA can be selected as the most promising ones for the reaction of PROX among the studied gold catalysts supported on ceria modified with reducible MeO_x. Both the catalytic activity and the selectivity over gold supported on mechanochemically prepared ceria doped by FeO_x and MnO_x are higher as compared to gold on undoped ceria. The observed dependence on the preparation method is the opposite of the previously obtained one with rare earths (RE) doped ceria supports. In Ref. [34] it has been established that the CP technique for the preparation of ceria modified with RE is more appropriate concerning gold catalysts for PROX than the MA method. The explanation was searched in the structure of the ceria support and the assumption of oxygen activation by chemisorption on surface anion vacancies in the vicinity of the border with gold particles, e.g. near to the CO molecule adsorbed on gold. The catalysts prepared by MA on one hand were double phased—supplementary to the modified ceria the separate phases of RE_2O_3 oxides, which are not reducible and not active in PROX, existed. On the other hand the modification by the MA method gives

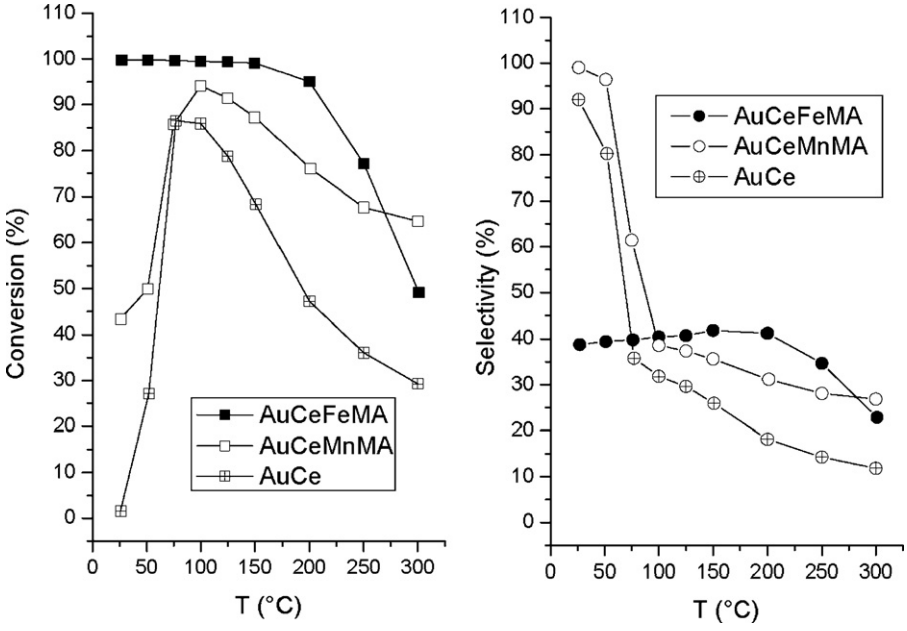

Fig. 13. Comparison between catalytic activity and selectivity of AuCeFeMA, AuCeMnMA and AuCe catalysts.

a larger amount of dopant on the ceria surface, thus causing a disturbance of the close contact between gold and ceria. The average size and the distribution of gold particles with all catalysts containing RE were very similar. Schubert et al., comparing the CO oxidation over not reducible ("inert") and reducible ("active") supports have concluded that the size of the gold particles seems to play only a secondary role in the case of such "active" supports [6]. In contradiction Luengnaruemitchai et al. [20] have reported that the PROX activity of Au/CeO_2 catalyst depends considerably on the size of gold. The prevailing opinion in the literature is that the mechanism of CO oxidation includes CO activation by adsorption onto Au^0. A high gold dispersion is needed in respect to this CO activation as the smooth surface of metallic gold does not adsorb CO, which is adsorbed only on steps, ages and corner sites [51]. The activation of oxygen has also to occur on gold using non-reducible supports. Very recently studying PROX over Au/Al_2O_3 Quinet et al. [52] have suggested a promotion effect of H_2 on CO oxidation because the simultaneous presence of O_2 and H_2 may stabilize $Au–O_xH_y$ species, which efficiently react with CO. However in the case of gold on reducible oxides, the majority of authors share the opinion that the oxygen activation occurs with the participation of supports, depending on their structure and properties. In the present study the HRTEM results showed the same average particle size (2.8–2.9 nm) for Fe- and Mn-containing samples prepared by both CP and MA methods. The difference in the size distribution of gold particles was not significant as well. In AuCeMnCP and AuCeMnMA catalysts the presence of gold particles with bigger size was obtained by XRD and then it was confirmed after detailed analyses of HRTEM images. However these Au particles have a very little impact onto the overall surface of gold. This means that again the differences in catalytic behaviour cannot be explained by the differences in the state of gold—the studied modified ceria supports lead to the stabilization of gold particles with similar low dispersion, responsible for CO adsorption. Schubert et al. [6] have concluded that for Au/Fe_2O_3 the dominant CO oxidation pathway involves adsorption on the support of mobile oxygen species in a molecular form, dissociation at the interface, and reaction on the gold particles and/or at the interface with CO adsorbed on the gold. The involvement of lattice oxygen of Fe_2O_3 in CO oxidation has been proposed [16,53,54] and the importance of oxygen vacancies caused by the change of the oxidative state of iron has been pointed out [55]. In addition to modified ceria some amount of separate phases of Fe_2O_3 and Fe_3O_4 were observed by HRTEM of the catalyst prepared by MA mode. In accordance, it was established on the basis of TPR results, that Fe^{3+} is the predominant part of Fe ions in CeFeCP. However, Fe ions in lower oxidative state exist in CeFeMA, e.g. the presence of both Fe_2O_3 and Fe_3O_4 could be supposed. The very high activity of AuCeFeMA up to 150 °C could be considered as a result of PROX activities of gold on modified with Fe ceria and gold on FeO_x phases.

When Mn-containing ceria support was prepared by MA method, the presence of MnO_2 and Mn_2O_3 was evidenced by HRTEM, TPR and XPS results. According to Wang et al., with respect to Au/MnO_x catalysts, the superior PROX activity of Au/Mn_2O_3 has been attributed to its unique redox properties and the facile formation of activated oxygen species on the surface [19]. In addition to gold on modified with Mn ceria, gold on MnO_x could also contribute to the PROX activity and selectivity. The high reducibility of CP catalyst, including the reduction both of ceria surface layers and $Mn^{4+} \rightarrow Mn^{2+}$ transition in the LT interval, could be the reason for lower selectivity within all studied temperature interval due to the enhanced H_2 oxidation. The conversion of CO over AuCeMnMA catalyst was 86% with selectivity of 61% at 77 °C, and 94% conversion and 39% selectivity at 100 °C. The results make the gold catalyst on doped with MnO_x ceria prepared by MA technique promising ones because of the interest for PROX especially at these fuel cells operating temperatures.

Unexpectedly, in the case of Co as dopant a very low catalytic activity and selectivity of AuCeCoMA sample in the interval 50–100 °C was obtained. A Co_3O_4 phase existence was suggested on the bases of XRD, TPR as well as XPS results. The eventual explanation could be connected to the assumption that the predominant part of gold is located on this phase and by this reason the ceria phase cannot be enough active in PROX. Concerning Au/Co_3O_4 phase—the intense TPR peak in the TPR pattern of AuCeCoMA sample as well as the presented in Fig. 12 curve for O_2 conversion suggest that the main process in those LT interval is H_2 oxidation accompanied with Co_3O_4 reduction. The CoO formation could suppress the PROX activity—Wang et al. [30] studying PROX over Au on prepared by sol–gel $CeO_2–Co_3O_4$ have shown the reduction to CoO as a reason for catalysts deactivation. The methane formation started over AuCeCoMA catalyst at temperature ≥150 °C can be explained with the deeper reduction to metallic cobalt. The catalytic behaviour of AuCeCoCP is similar to that of gold on ceria with CP incorporated Fe or Mn ions; the catalytic activity is lower but the selectivity is higher compared to that of AuCeFeCP and AuCeMnCP. It has to be mentioned a methane formation at temperature ≥200 °C registered with AuCeCoCP catalyst.

5. Conclusions

On the basis of the obtained results, the gold catalysts on ceria supports, mechanochemically modified with FeO_x and MnO_x, can be selected as the most promising ones for PROX among the studied catalysts.

The differences in the catalytic behaviour cannot be explained by differences in gold dispersion (a high dispersion of gold particles, similar for Fe- and Mn-containing catalysts prepared by CP or MA methods was established by HRTEM). The support structure, depending on the dopant nature and on the preparation technique, determines the redox and catalytic properties. When co-precipitation method was applied a deeper insertion of dopant in ceria structure occurs, while the mechanochemical activation leads to the formation of separate dopant oxide phases (XRD and HRTEM data). In the case of MA preparation, beside the activity of gold on ceria (modified with Fe and Mn) there is also activity by gold on FeO_x and MnO_x phases, which also contributes to the high PROX activity and selectivity. Co-containing MA catalyst exhibited a very low PROX activity. The observed low selectivity could be due to the H_2 oxidation (accompanied by Co_3O_4 reduction to the inactive CoO) as well as methane formation (with participation of Co reduced to metallic state).

Acknowledgments

This research study has been performed in the framework of a D36/003/06 COST program. L.I., I.I., A.M. and D.A. gratefully acknowledge the support provided by the National Science Fund, Ministry of Education and Sciences of Bulgaria (project TK-X-1709). The Bulgarian and Italian teams as well as Bulgarian and Polish authors are also indebted to the bilateral collaboration supported by CNR, respectively, Polish Academy of Science, and Bulgarian Academy of Science. R.Z. acknowledges PUNTA (IMPULSA 01), PAPIIT IN106507, IN108310 and CONACYT 55154 project for the financial support.

References

[1] D. Cameron, R. Holliday, D. Thompson, J. Power Sources 118 (2003) 298, and references therein.
[2] M. Haruta, S. Tsubota, T. Kobayashi, H. Kageyama, M. Jenet, B. Delmon, J. Catal. 144 (1993) 175.
[3] R.M. Torres Sanchez, A. Ueda, K. Tanaka, M. Haruta, J. Catal. 168 (1997) 125.
[4] R.J.H. Grisel, B.E. Nieuwenhuys, J. Catal. 199 (2001) 48.

[5] S. Kandoi, A.A. Gokhale, L.C. Grabow, J.A. Dumesic, M. Mavrikakis, Catal. Lett. 93 (2004) 93.
[6] M.M. Schubert, S. Hackenberg, A.C. van Veen, M. Muhter, V. Pizak, R.J. Behm, J. Catal. 197 (2001) 113.
[7] S. Carretin, P. Concepcion, A. Corma, J.M. Lopez Nieto, V.F. Puntes, Angew. Chem. Int. Ed. 43 (2004) 2538.
[8] B.K. Min, C.M. Friend, Chem. Rev. 107 (2007) 2709.
[9] A.M. Visko, A. Bonato, C. Milone, S. Galvagno, React. Kinet. Catal. Lett. 62 (1997) 219.
[10] M.J. Kahlich, H.A. Gasteiger, R.J. Behm, J. Catal. 182 (1999) 430.
[11] M.M. Schubert, V. Pizak, J. Garche, R.J. Behm, Catal. Lett. 76 (2001) 143.
[12] G. Avgouropoulos, T. Ionnides, C. Papadopoulou, J. Batista, S. Hocevar, H.K. Matralis, Catal. Today 75 (2002) 157.
[13] L. Guczi, D. Horvath, Z. Paszti, G. Peto, Catal. Today 72 (2002) 101.
[14] M.M. Schubert, A. Venugopal, M.J. Kahlich, V. Plzak, R.J. Behm, J. Catal. 222 (2004) 32.
[15] A. Luengnaruemitchai, D.T.K. Thoa, S. Osuwan, E. Gulari, Int. J. Hydrogen Energy 30 (2005) 981.
[16] S. Scire, C. Crisafulli, S. Minico, G.G. Condorelli, A. Di Mauro, J. Molec. Catal. A: Gen. 284 (2008) 24.
[17] G.B. Hoflund, S.D. Gardner, D.R. Schyer, B.T. Upchurch, E.J. Kielin, Appl. Catal. B. Environ. 6 (1995) 117.
[18] S.J. Lee, A. Gavriilidis, Q.A. Pankhurst, A. Kyek, F.E. Wanger, P.C.L. Wong, K.L. Yeung, J. Catal. 200 (2001) 298.
[19] L.-C. Wang, X.-S. Huang, Q. Liu, Y.-M. Liu, Y. Cao, H.-Y. He, K.-N. Fan, J.-H. Zhuang, J. Catal. 259 (2008) 66.
[20] A. Luengnaruemitchai, S. Osuwan, E. Gulari, Int. J. Hydrogen Energy 29 (2004) 429.
[21] G. Panzera, V. Modafferi, S. Candamano, A. Donato, F. Rusteri, P.L. Antonucci, J. Power Sources 135 (2004) 177.
[22] O. Goerke, P. Pfeifer, K. Shubert, Appl. Catal. A: Gen. 263 (2004) 11.
[23] W.L. Deng, J.D. Jesús, H. Saltsburg, M. Flytzani-Stephanopoulos, Appl. Catal. A: Gen. 291 (2005) 126.
[24] F. Arena, P. Famulari, G. Trunfio, G. Bonura, F. Frusteri, L. Spadaro, Appl. Catal. B: Environ. 66 (2006) 81.
[25] G. Avgouropoulos, J. Papavasiliou, T. Tabakova, V. Idakiev, T. Ionnides, Chem. Eng. J. 124 (2006) 41.
[26] L.-H. Chang, N. Sasirekha, B. Rajesh, Y.-W. Chen, Sep. Purif. Technol. 58 (2007) 211.
[27] L.-H. Chang, N. Sasirekha, B. Rajesh, Y.-W. Chen, W.-J. Wang, Ind. Eng. Chem. Res. 45 (2006) 4927.
[28] Y.-B. Tu, J.-Y. Luo, M. Meng, G. Wang, J.-J. He, Int. J. Hydrogen Energy 34 (2009) 3743.
[29] H. Wang, H.Q. Zhu, Z.F. Qin, G.F. Wang, F.X. Liang, J.G. Wang, Catal. Commun. 9 (2008) 1487.
[30] H. Wang, H. Zhu, Z. Qin, G.F. Wang, F. Liang, G. Wang, J. Wang, J. Catal. 264 (2009) 154.
[31] A. Trovarelli, Catal. Rev. Sci. Eng. 38 (1996) 439.
[32] G. Avgouropoulos, M. Manzoli, F. Boccuzzi, T. Tabakova, J. Papavasiliou, T. Ioannides, V. Idakiev, J. Catal. 256 (2008) 237.
[33] M. Manzoli, G. Avgouropoulos, T. Tabakova, J. Papavasiliou, T. Ioannides, F. Boccuzzi, Catal. Today 138 (2008) 239.
[34] L. Ilieva, G. Pantaleo, I. Ivanov, R. Zanella, A.M. Venezia, D. Andreeva, Int. J. Hydrogen Energy 34 (2009) 6505.
[35] E.J. Mittemeijer, P. Scardi (Eds.), Diffraction Analysis of the Microstructure of Materials, Springer Series in Material Science, vol. 68, Springer-Verlag, Berlin/Heidelberg, 2004.
[36] K.M. Ryan, J.P. McGrath, R.A. Farrell, W.M. O'Neill, C.J. Barnes, M.A. Morris, J. Phys. Condens. Matter 15 (2003) L49–L58.
[37] N. Kotzev, D. Shopov, J. Catal. 22 (1971) 297.
[38] D.A.M. Monti, A. Baiker, J. Catal. 83 (1983) 323.
[39] B. Harrison, A.F. Diwell, C. Hallett, Plat. Met. Rev. 32 (1988) 73.
[40] D. Andreeva, V. Idakiev, T. Tabakova, L. Ilieva, P. Falaras, A. Bourlinos, A. Travlos, Catal. Today 72 (2002) 51.
[41] L. Ilieva, D. Andreeva, A. Andreev, Therm. Acta 292 (1997) 169.
[42] E.R. Stobe, B.A. de Boer, J.W. Geus, Catal. Today 47 (1999) 161.
[43] L. Ilieva, G. Munteanu, D. Andreeva, Bulg. Chem. Commun. 30 (1998) 378.
[44] L. Liota, Q. Guo, Y. Liu, Appl. Catal. B: Environ. 82 (2008) 19.
[45] M.G. Sanchez, J.L. Gazquez, J. Catal. 104 (1987) 120.
[46] A. Laachir, V. Perrichon, A. Bardi, J. Lamotte, E. Catherine, J.C. Lavalley, J. El Faallah, L. Hilaire, F. le Normand, E. Quemere, G.N. Sauvion, O. Touret, J. Chem. Soc. Faraday Trans. 87 (1991) 1601.
[47] D. Andreeva, I. Ivanov, L. Ilieva, J.W. Sobczak, W. Lisowski, unpublished results.
[48] A. De Stefanis, S. Kaciulis, L. Pandolfi, Micropor. Mesopor. Mater. 99 (2007) 140.
[49] NIST X-ray Photoelectron Spectroscopy Database, V. 4.0, 2008, http://srdata.nist.gov/xps/.
[50] Q. Guo, Y. Liu, Appl. Catal. B: Environ. 82 (2008) 19, and references therein.
[51] F. Boccuzzi, A. Chiorino, M. Manzoli, P. Lu, T. Akita, S. Ishikava, M. Haruta, J. Catal. 187 (1999) 343.
[52] E. Quinet, L. Piccolo, F. Morfin, P. Avenier, F. Diehl, V. Caps, J.-L. Rousset, J. Catal. 268 (2009) 384, and references therein.
[53] A.K. Tripathi, V.S. Kamble, N.M. Gupta, J. Catal. 187 (1999) 332.
[54] N.M. Gupta, A.K. Tripathi, J. Catal. 187 (1999) 343.
[55] D. Horvath, L. Toth, L. Guczi, Catal. Lett. 67 (2000) 117.